International Journal of Environmental Science and Technology (2025) 22:10049–10066
https://doi.org/10.1007/s13762-025-06492-4

ORIGINAL PAPER

Rapid adsorption of methylene blue by synthesizing zinc oxide nanoparticles from *Ocimum basilicum* L. waste

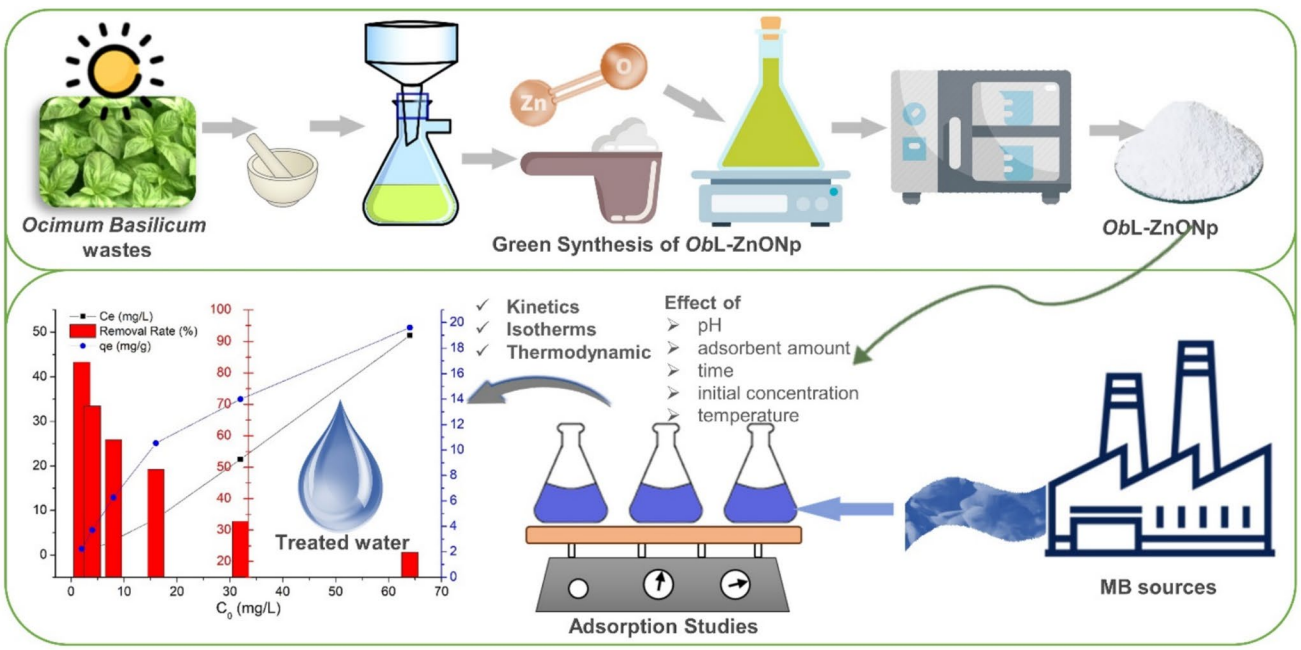
T. Turna[1] · A. Solmaz[2] · A. Baran[3]

Received: 3 October 2024 / Revised: 7 December 2024 / Accepted: 15 April 2025 / Published online: 15 May 2025
© The Author(s) 2025

Abstract

In this study, zinc oxide nanoparticles (ZnONp) were synthesized from *Ocimum basilicum* L. (*Ob*L-ZnONp) plant wastes by green synthesis method to remove methylene blue (MB) dye, which has toxic effects on the environment. In batch adsorption studies, the effects of pH (3–11), *Ob*L-ZnONp amount (0.0312–1.25 g/L), time (0–30 min), initial MB concentration (2–64 mg/L) and temperature (25–45 °C) were tested to determine the adsorption mechanism. The obtained results were tested with Pseudo first order (PFO), Pseudo second order (PSO), Elovich and Intraparticle diffusion kinetic models and evaluated in Freundlich, Langmuir, Temkin and Dubinin-Radushkevich isotherm models. Also 6 different error functions were used to interpret the results. Additionally, the morphological properties of the synthesized *Ob*L-ZnONp were characterized by Fourier transform infrared (FTIR) spectroscopy, scanning electron microscopy (SEM) and energy dispersive X-ray (EDX) analysis. In addition, desorption tests were also performed. According to the obtained results, the most suitable kinetic and isotherm models were determined as PSO (R^2: 0.999) and Freundlich (0.991), respectively. In addition, while more than 90% removal efficiency was achieved in 4 min, the maximum adsorption amount was determined as 21.41 mgMB/g*Ob*L-ZnONp. This study determined that Np synthesized at low cost was quite effective in MB removal.

Graphical abstract



Editorial responsibility: Samareh Mirkia.

Extended author information available on the last page of the article

Keywords Green synthesis · *Ocimum basilicum* L. wastes · Nanoparticle · Methylene blue · Rapid adsorption

Introduction

Today, due to the uncontrolled increase in urbanization, excessive amounts of industrial wastewater are produced. The produced wastewater contains some toxic pollutants such as heavy metals, dyes and medical wastes, and these waters are freely released into the aquatic ecosystem without any pre-treatment (Shah et al. 2024). The biggest challenges to sustainable development, which is one of the most effective approaches to solving these problems, are the increasing demand for accessible and clean water resources and the inappropriate discharge of pollutants into existing water resources (Aiman Khan et al. 2022). The most important of these difficulties is the uncontrolled discharge of domestic and industrial wastewater into the receiving environment. One of the sectors with the highest share in industrial pollution is the textile sector. A wide variety of synthetic materials are widely used in the textile industry, which associates the industry with excessive chemical use in addition to water and energy (Hole and Hole 2019). Many different types of dyes are widely used in various industries, especially in textiles, food, paper, plastic, and metal industries (Lellis et al. 2019). MB is a dye used extensively in dyeing cotton, medicine, wood, paper, and silk. It is also a toxic thiazine group cationic dye that can form a stable solution with water at room temperature. This dye is a chemical compound with a heterocyclic aromatic structure and is highly resistant to light and water (Russo et al. 2016; Said et al. 2023). In addition, MB can cause eye burns, which can lead to irreversible damage to human and animal eyes. Inhalation can cause respiratory problems. And exposure to MB dye through water use can cause health problems such as excessive sweating, shortness of breath, tissue necrosis, disorientation, dermatitis, cyanosis, nausea, difficulty breathing, vomiting, and eye burning (Ponnusami et al. 2008). For these reasons, pollutants with toxicological properties such as MB dye must be treated before being released into the environment.

Therefore, there is a need to develop treatment methods that are environmentally sustainable, innovative and do not cause toxicological effects. Water treatment with nanotechnology has recently become an interest in researchers. Thanks to the advancement of nanotechnology, new opportunities have been created for the treatment of water pollutants. Nanotechnology-based treatment options are much more effective than classical approaches due to their high surface area, smaller dimensions, high volume ratio and improved chemical properties (Nandan et al. 2023). Especially to adsorb chemical pollutants, nanoparticles with high affinity organic or inorganic content are used more frequently. These nanoparticles are very effective in removing various pollutants. They have optimum absorbent properties with their large surface area, strong catalytic ability, small size, and high reactivity (Punia et al. 2021).

Metal–metal oxide nanoparticles in water treatment have many engineering applications including the removal of pollutants (Gómez-Pastora et al. 2014). The surface of metal nanoparticles contains special functional groups for the effective removal of inorganic and organic pollutants from industrial wastes. These metallic nanoparticles contain chemicals such as gold, silver, titanium oxide, zinc oxide, selenium, copper, and copper oxide. They attract the attention of researchers due to their unique characteristics (Salem et al. 2020; Zhang et al. 2023; Kaval and Hoşgören 2024). Numerous processes such as chemical, physical, and photochemical reduction, electrochemical modification and microwave assisted metal nanoparticles are widely used for their preparation and stabilization. However, there are several problems associated with these processes due to the use of toxic materials as reducing agents in the production processes and their application in biological systems (Ocsoy et al. 2017; Jamkhande et al. 2019). To overcome the toxicological problems that arise because of these production processes, it was necessary to use more environmentally friendly methods in the synthesis phase. Thereupon, the green production method was started to be used to produce nanomaterials. In this method, non-toxic and natural substances such as fungi, bacteria and plant extracts were used. These non-toxic substances used in the production processes serve as stabilizers, coverers, and reducers in the production phase (Chandra et al. 2020; Chaudhary et al. 2023).

The green synthesis method used for the preparation of metal oxide nanoparticles is an environmentally friendly, safe, and inexpensive process (Shaghaghi et al. 2023). In a study, various plant seed extracts were used to produce ZnO-NPs by green synthesis method. It was revealed that the synthesized ZnO NPs could act as active antimicrobial agents (Perveen et al. 2020). In a different study, ZnO NPs were produced by green synthesis method using *artocarpus heterophyllus* leaf extract and it was reported that 90% efficiency was achieved in the removal of Congo red (Vidya et al. 2017). In summary, nanoparticles produced using green synthesis method are qualified nanomaterials used in water and wastewater treatment due to their important properties such as strong oxidation property and wide-bandwidth near-UV wavelength. ZnO NPs are

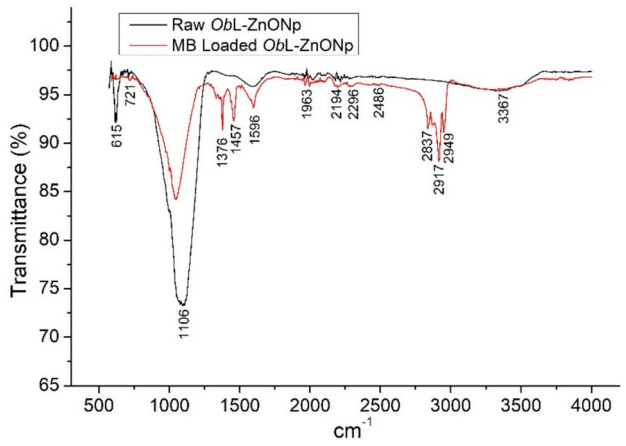


Fig. 1 FTIR diagram of *Ob*L-ZnONp, black line: raw, red line: MB loaded

environmentally friendly as they are compatible with living biomass in water and wastewater (Madhumitha et al. 2016).

In this study, *Ob*L-ZnONp was synthesized from OB plant wastes by green synthesis method and SEM–EDX and FTIR analyses were performed. MB dye in aqueous solution was removed with the *Ob*L-ZnONp obtained. In addition, the effects of pH, initial dye concentration, adsorbent amount, time and temperature were carried out by adsorption tests in the study. The obtained results were examined with kinetic models (PFO, PSO, Elovich and Intraparticle diffusion) and isotherm models (Freundlich, Langmuir, Temkin and Dubinin-Radushkevich) and 6 different error functions.

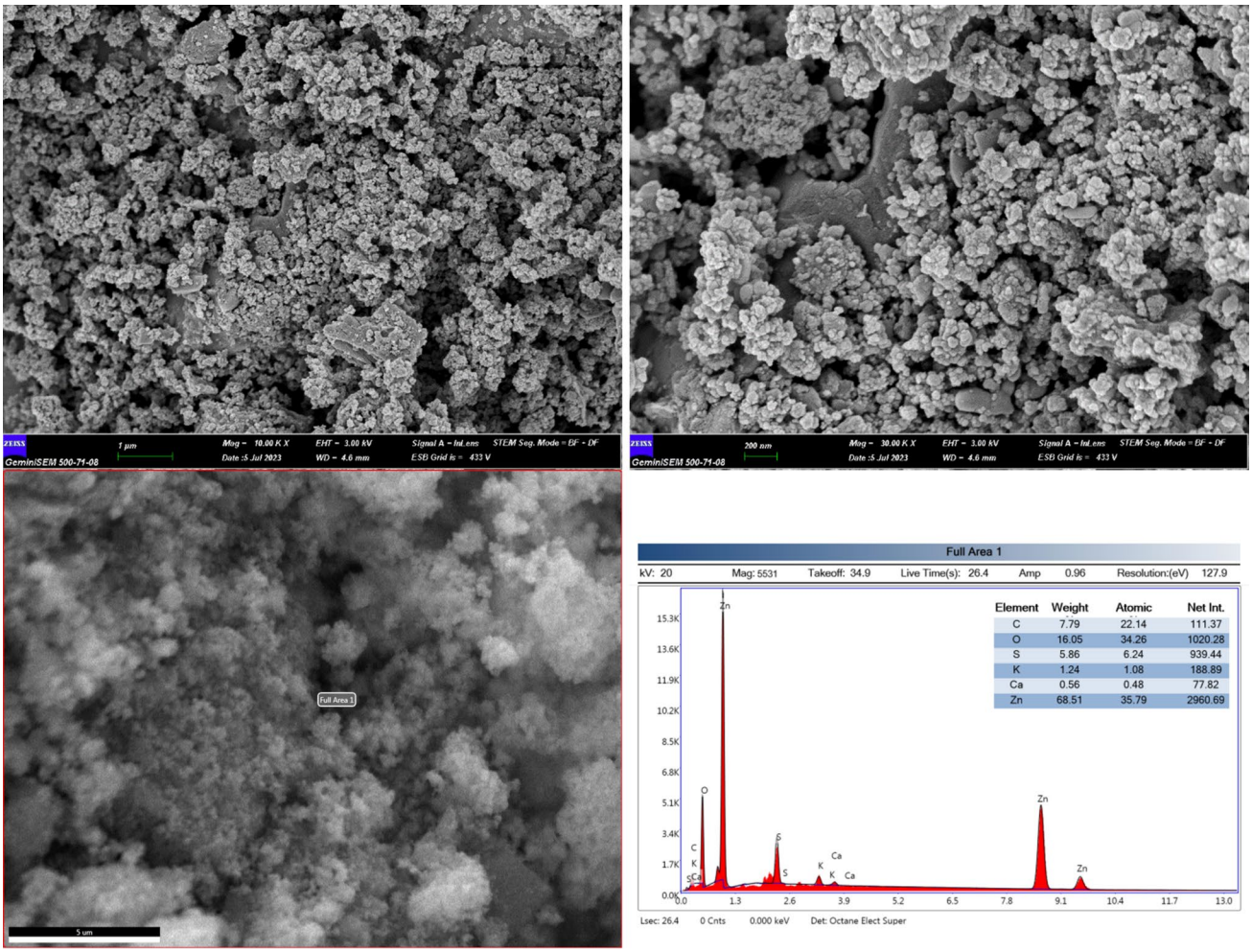


Fig. 2 SEM–EDX diagram of MB dye on *Ob*L-ZnONps before reaction

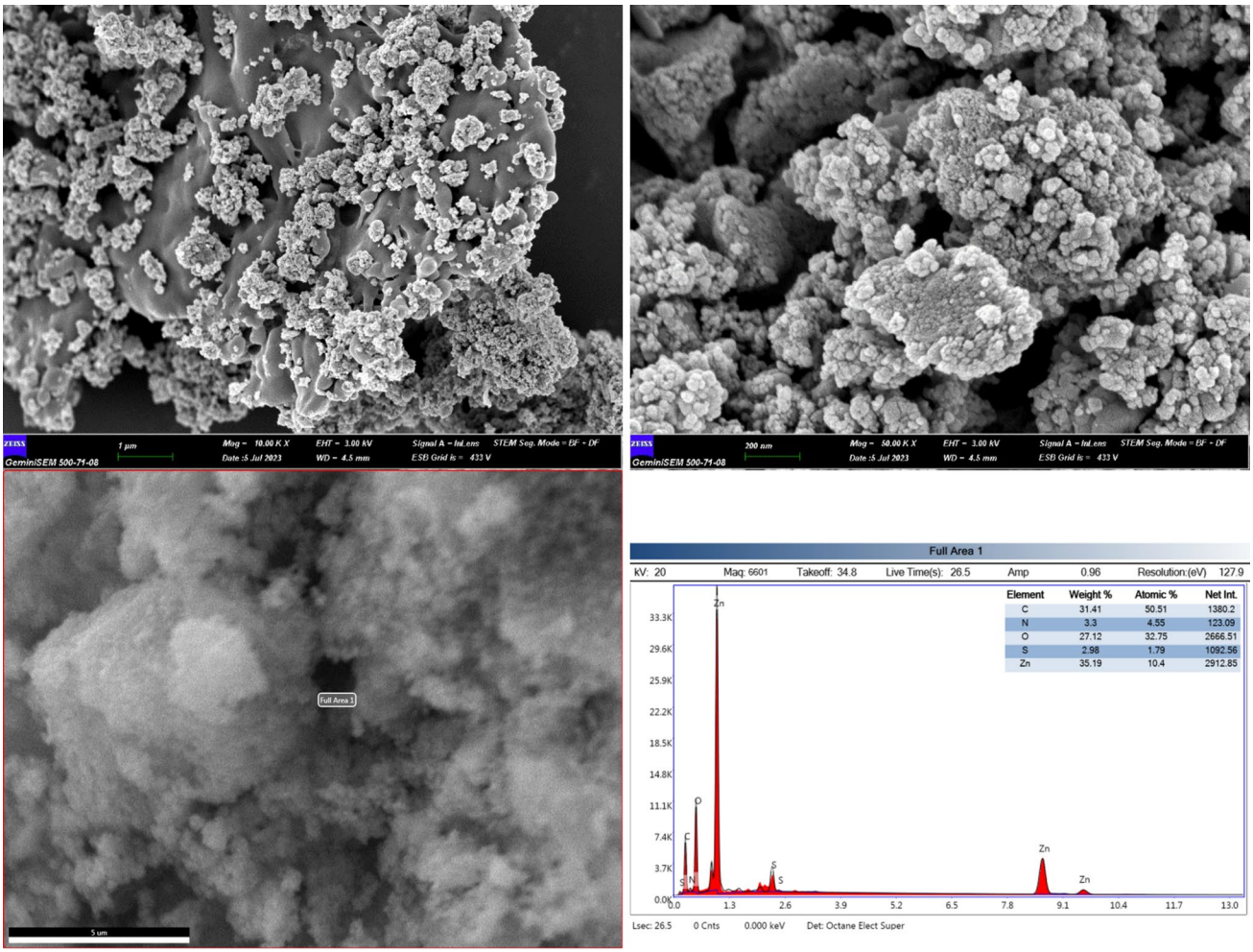


Fig. 3 SEM–EDX diagram of MB dye on *Ob*L-ZnONps after reaction

Materials and methods

Chemicals

Distilled water was used in the preparation of solutions in experimental studies. Also powder zinc oxide (ZnO, 81.39 g/mol, ≥ 99.0%, Merck), zinc nitrate hexahydrate ($Zn(NO_3)_2.6H_2O$, 327 g/mol, 98%, Sigma-Aldrich), powder methylene blue ($C_{16}H_{18}ClN_3S.xH_2O$, 319.85 g/mol (anhydrous)), pellet NaOH (40.00 g/mol), and liquit H_2SO_4 (98.08 g/mol) was used.

Product of *Ob*L-ZnONp

*Ob*L-ZnONp synthesis processes are specified in the study of Solmaz et al. (2024). In this context, plants collected from Mardin (Turkey) province in the summer season were first washed with tap water and then with pure water. The waste stems of the plant were dried in the shade and turned into powder. Then, 30 g of powder was added to 200 mL of distilled water and mixed at 85 °C for 1 h (Shaban et al. 2024). The solution that reached room temperature was filtered through filter paper. The volume of the filtrate is 150 mL. After than added to 300 mL of 100 mM concentration $Zn(NO_3)_2.6H_2O$ solution and treated at 80 °C for 45 min. The pH of the solution was brought to 9.4 and the stirring was continued for another half hour until the solution color turned light brown by magnetic stirrer (Al-darwesh et al. 2024). At the end of the process, centrifugation was performed. The pellet was washed 7 times with distilled water. After then pellet part was first dried at 65 °C and then kept at 500 °C for 1 h for calcination. The solid agate that reached room temperature was pounded in a mortar. The resulting powder was stored in a falcon tube at room temperature (Solmaz et al. 2024).

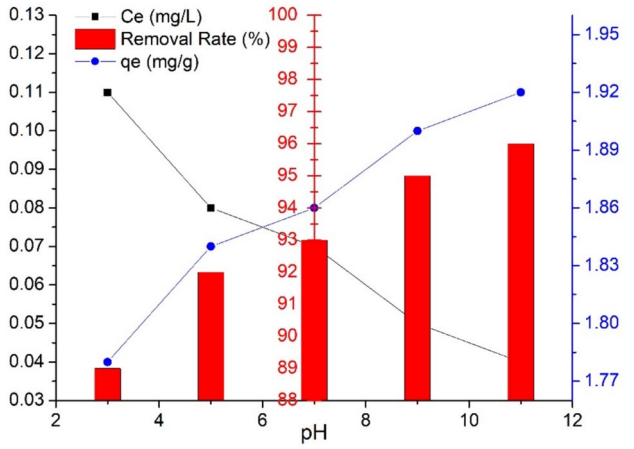


Fig. 4 Effect of pH on the adsorption of MB dye onto *Ob*L-ZnONp

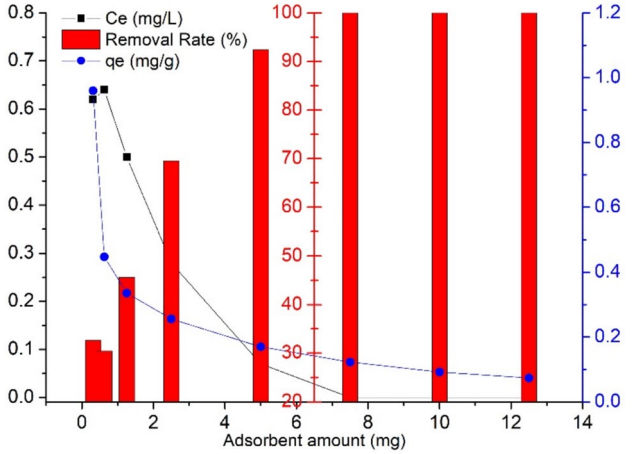


Fig. 5 Effect of *Ob*L-ZnONp amount on the adsorption of MB dye onto *Ob*L-ZnONp

Adsorption studies

An orbital shaker (Heidolp, Unimax1010, Germany) was used in adsorption experiments. The tests were carried out at a speed of approximately 200 rpm. A stock solution of 1000 mg/L concentration of MB dye was prepared and a calibration curve was created at 664 nm wavelength in a UV–Vis spectrophotometer (Hach DR6000) by making dilutions at certain rates from this solution. The concentration of the measured solution was found according to the calculation made according to the equation $y = 0.2097x + 0.0131$ (R^2: 0.9996). The results were interpreted according to Eqs. (1) and (2).

$$R(\%) = \frac{C_0 - C_e}{C_0} \times 100 \tag{1}$$

$$q_e = \frac{(C_0 - C_{e)} \times V}{m} \tag{2}$$

In Eq. (1), the R term defines the removal efficiency in terms of %, while the C_0 and C_e expressions shown in both equations define the concentration of MB dye at the beginning of the reaction and at equilibrium in mg/L. In addition, the q_e term presented in Eq. 2 defines the amount of MB dye removed per unit adsorbent in mg/g, while the V term represents the volume of the solution in L, and the m term represents the amount of *Ob*L-ZnONp in g.

The effect of environmental parameters on the adsorption of MB dye onto *Ob*L-ZnONs was investigated. In this context, in order to determine the effect of pH, 5 mg *Ob*L-ZnONp was added to 5 different 10 mL test tubes with an initial pH of 3–11 and an initial MB dye concentration of 1 mg/L at room temperature and left to react for 30 min. Then, it was centrifuged at 4100 rpm for 5 min and the MB dye concentration in the upper phase water was read, thus determining the optimum pH. Then, in order to determine the effect of the amount of *Ob*L-ZnONp on the removal of MB dye, *Ob*L-ZnONp was added in amounts ranging from 0.3125 to 12.5 g to 8 different 10 mL test tubes with an initial MB dye concentration of 1 mg/L at neutral pH. and at the end of the experiment at the end of 30 min, after centrifugation, the MB dye concentration in the upper phase water was measured and the optimum *Ob*L-ZnONp amount was found. Then, in order to see the effect of time and to make kinetic calculations, 37.5 mg *Ob*L-ZnONp was added to a 50 mL beaker with an initial MB dye concentration of 1 mg/L and samples were taken with a 0.45-micron syringe filter at certain times and the MB dye concentration was read. In addition, in order to see the effect of the initial MB dye concentration on the adsorption of MB dye onto *Ob*L-ZnONps, 7.5 mg

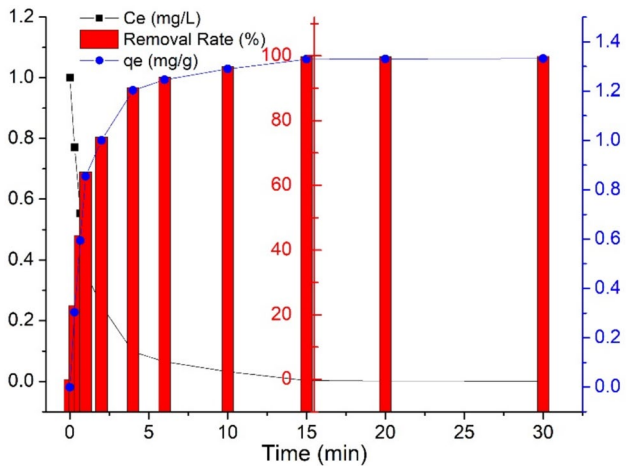


Fig. 6 Effect of contact time on the adsorption of MB dye onto *Ob*L-ZnONp

*Ob*L-ZnONp was added to each of the tubes containing MB dye at varying concentrations between 2 and 64 mg/L in 7 different test tubes, each with a volume of 10 mL, and centrifugation was performed after 30 min and the MB dye concentrations in the upper phase water were read. In addition, to determine the effect of temperature and therefore to examine thermodynamically, 0.1 g of *Ob*L-ZnONp was added to each of 3 different solutions with a volume of 50 mL having a concentration of 3.5 mg/L MB and experiments were conducted at 298, 308 and 318 K. At the end of the period, centrifugation was performed, and the MB concentration was read.

For kinetic evaluation of numerical data obtained from batch adsorption tests, linear forms of PFO, PSO, Elovich and Intra-particle diffusion models were used. Also, linear forms of Freundlich, Langmuir, Temkin and Dubinin–Redushkevich isotherm models were used for isotherm calculations.

Error function test describing

Some error functions were used to identify the numerical data derived from laboratory data and adsorption models produced from experimental studies on the adsorption of MB dye on *Ob*L-ZnONp. The error sum of squares (SSE) error function, which is defined as the sum of the squares of the difference between the values calculated from the models and the values obtained in the laboratory, is presented in Eq. (3). In addition, the model Sum of Absolute Errors (SAE), which expresses the sum of the squares of the absolute errors between the results obtained in the laboratory and the results obtained from the models, is presented in Eq. (4). In addition, the average relative errors (ARE) function, which is defined as the sum of the absolute values of the difference between the results obtained from the models and the results obtained in the laboratory divided by the laboratory results, is presented in Eq. (5) (Ncibi 2008; Sreńscek-Nazzal et al. 2015).

$$SSE = \sum (q_{e,cal} - q_{e,exp}) \tag{3}$$

$$SAE = \sum_{i=1}^{n} \left| q_{e,exp} - q_{e,cal} \right| \tag{4}$$

$$ARE = \frac{1}{n} \sum_{i=1}^{n} \left| \frac{q_{e,cal} - q_{e,exp}}{q_{e,exp}} \right| \tag{5}$$

In addition to these, Hybrid fractional error function (HYBRID) error function is presented in Eq. (6), Marquardt's percent standard deviation (MPSD) error function is presented in Eq. (7) and Non-linear Chi-Square test (X^2) is presented in Eq. (8) (Ncibi 2008; Foo and Hameed 2010).

$$HYBRID = \frac{1}{N-P} \sum \left| \frac{q_{e,exp} - q_{e,cal}}{q_{e,exp}} \right| \tag{6}$$

$$MPSD = \sqrt{\frac{\sum \left| (q_{e,exp} - q_{e,cal})/q_{e,exp} \right|^2}{N-P}} \tag{7}$$

$$X^2 = \sum \frac{(q_{e,exp} - q_{e,exp})^2}{q_{e,cal}} \tag{8}$$

Results and discussion

Characteristic of *Ob*L-ZnONp

According to the obtained XRD results, hexagonal crystal pattern of *Ob*L-ZnONp was investigated according to Bragg's angler. Also, it was reported that the dimensions of the nanoparticles were determined as 30.39 nm according to the Debye-Scherre equation. On the other hand, according to the BET analysis, the surface area of the NPs was reported as 13.826 m^2/g and the total pore diameter was reported as 0.0475 cm^3/g. In addition, in the DLS-Zetasizer analysis, the average size distribution of the nanoparticles was reported as 10–40 nm and the zeta potential was reported as −22.1 mV. In addition, UV–Vis spectroscopy of *Ob*L-ZnONp was examined and it was reported that it gave a peak at 373 nm wavelength at 4 different concentrations. On the other hand, TGA-DTA analysis of the material was performed and it was

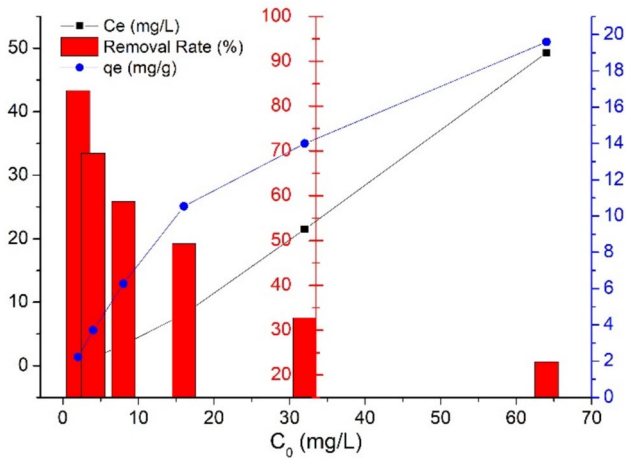


Fig. 7 Effect of initial MB concentration on the adsorption of MB dye onto *Ob*L-ZnO Np

Table 1 Summary of the calculated kinetic parameters in the adsorption of MB onto *Ob*L-ZnONp

Kinetic models	Parameters	R^2	SSE	SAE	ARE	HYBRID	MPSD	X^2
PFO	$k_1 = 0.052$	0.906	0.950	2.36	43.93	61.49	0.995	1.18
PSO	$k_2 = 1.011$ $q_e = 1.374$	0.999	0.020	0.332	8.49	6.37	0.972	0.046
Elovich	$\beta = 4.176$ $\alpha = 5.346$	0.905	0.140	1.031	18.42	10.38	0.978	0.174
Intra-particle diffusion	$k_i = 0.174$ $a = 0.61$	0.657	0.391	1.69	36.19	21.27	0.985	0.739

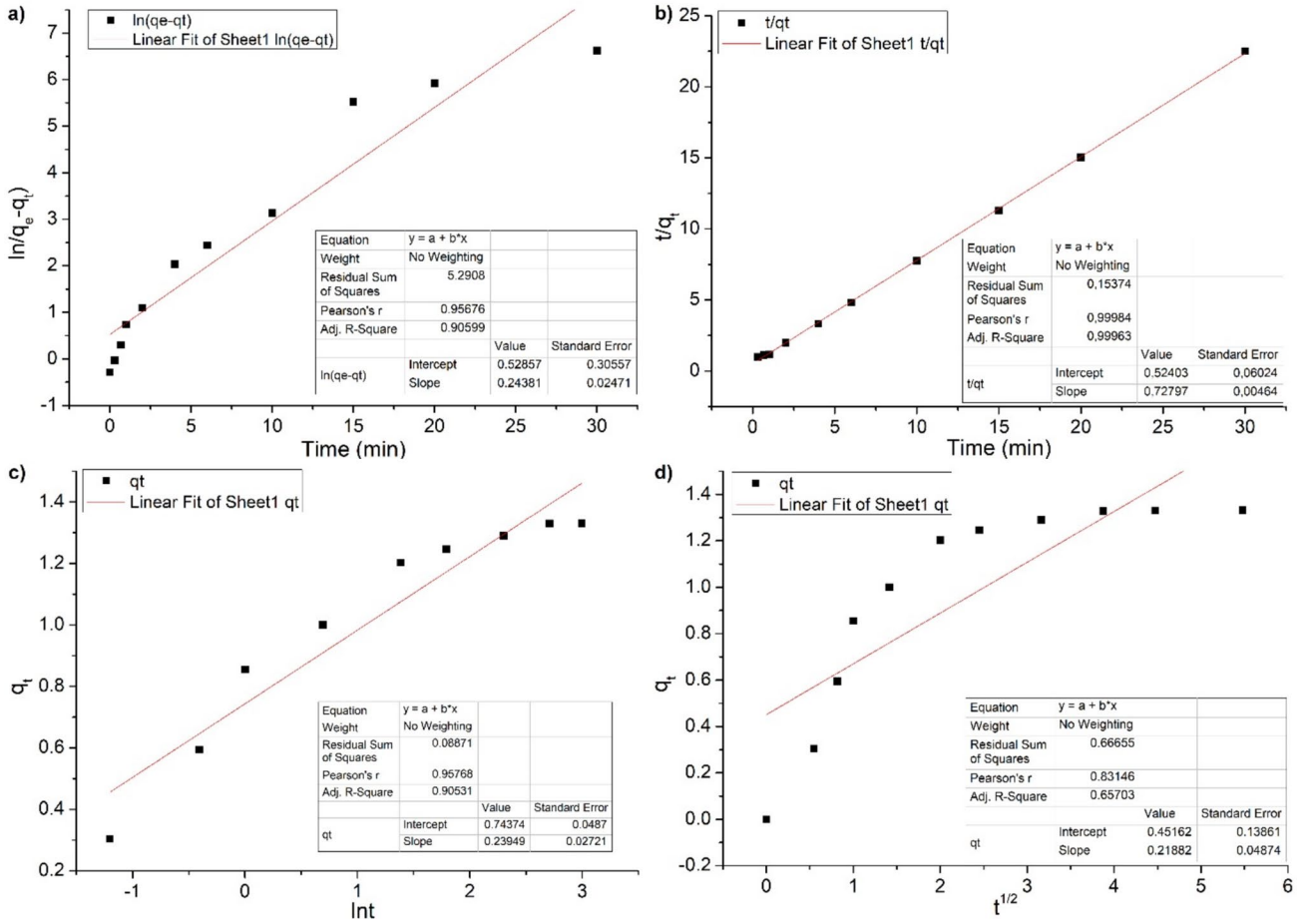


Fig. 8 Linear regression curves of the kinetic models studied (**a** PFO, **b** PSO, **c** Elovich, **d** Intra-particle diffusion)

reported that the mass loss was determined as 33% at 75 °C (Solmaz et al. 2024).

FTIR spectroscopy

Figure 1 presents the FTIR spectra of the raw and MB-loaded forms of *Ob*L-ZnONp. Accordingly, various determinations were made according to the possible changes in functional groups. Stretching vibrations occurring at 3367 cm^{-1}, 2949 cm^{-1}, 2917 cm^{-1}, 2837 cm^{-1}, 2286 cm^{-1}, 2194 cm^{-1}, 1963 cm^{-1}, 1596 cm^{-1}, 1457 cm^{-1}, 1376 cm^{-1}, 1106 cm^{-1}, 721 cm^{-1}, 615 cm^{-1} in the data showed that *Ob*L-ZnONp's are the functional groups responsible for the removal of MB by adsorption. It shows that alcohol, amine, aliphatic, aromatic alcohols, carbonyl groups are effective in adsorption. It was determined that the frequency changes due to stretching vibrations occurring in the range of 3367 cm^{-1}–2837 cm^{-1} were between hydroxyl (O–H) and aliphatic (C–H) groups (Manojkumar et al. 2023; Omran 2023). It was related to the C≡C stretching vibration observed at 2194 cm^{-1}, and the shifts in the range of

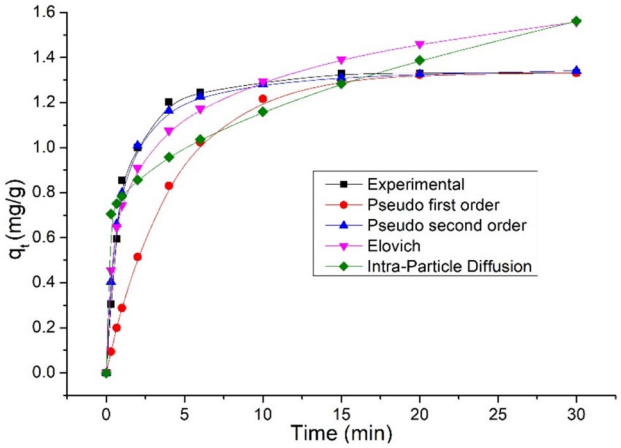


Fig. 9 q_e values of each kinetic model and laboratory results versus time.

2286 cm^{-1}–1963 cm^{-1} were related to carbonyl (–COOH) groups. It was evaluated that the stretching vibration mode was due to the C–C and N–H stretching mode as a result of the stretching vibrations occurring at 1106 cm^{-1} with the changes between 1596 cm^{-1} and 1376 cm^{-1}, together with the stretching vibration mode of aromatic alcohol (C–O–H) and amine groups, and the C–N stretching. It was determined that the frequency changes observed at 721 cm^{-1} and 615 cm^{-1} belonged to characteristic ZnO nanoparticles (Abdelsattar et al. 2023; Villegas-Fuentes et al. 2023).

SEM and EDX

The morphological appearances and elemental compositions of *Ob*L-ZnONps before and after adsorption were evaluated using SEM microscopy and EDX profiles given in Figs. 2 and 3. In the SEM microscopy images, it is seen that *Ob*L-ZnONps mostly have spherical morphology (Amin et al. 2023; Shochah and Jabir 2024). In the EDX profiles, the presence of C, O, K, Ca, S, N and Zn elements is seen. Strong peaks belonging to Zn and O elements indicate the presence of *Ob*L-ZnONps. In the EDX profiles before and after the reaction, it is seen that there are decreases and increases especially on the weight % and atom % of C, O, S, K, S elements. It is seen that K and Ca elements are not reflected in the profile after the reaction, instead, the peaks belonging to N element are seen despite not being present before the reaction. These changes reflected in the profile are thought to be due to the adsorption of MB by *Ob*L-ZnONps (Albarakaty et al. 2023; Manojkumar et al. 2023; Elsamra et al. 2024).

Adsorption of MB dye onto *Ob*L-ZnONp

Effect of different environment

Effect of pH The effect of pH on the adsorption of MB dye onto *Ob*L-ZnONp is quite high. An increase or decrease in pH causes variability in functional groups. This variability may affect the adhesion between the pollutant (MB) and the adsorbent (*Ob*L-ZnONp). The results obtained from the experimental studies conducted to determine this effect are presented in Fig. 4.

As can be seen from the figure, an increase in the removal rate of MB dye is detected when the pH of the medium increases from acidic to basic. For example, while the q_e value was 1.78 mg/g at pH 3, when it reached pH 7, the q_e value reached 1.86 mg/g, and was calculated as 1.92 at pH 11. When the removal efficiencies were examined, the efficiency was calculated as 89% at pH 3, while this value was 93% at pH 7 and 96% at pH 11. Since the functional groups are protonated in acidic conditions and the hydrogen ions and MB dye ions compete, the removal efficiency in acidic environments is relatively low compared to other environments (Zhang et al. 2013). However, it is clear that increasing the pH to basic environments increases the efficiency but does not cause a very high increase. In this context, it would be appropriate to choose neutral pH as the optimum pH since it provides benefits in terms of base consumption. When the literature is examined, it has been reported that neutral pH rather than acidic pH provides higher efficiency in the adsorption of MB dye onto magnesium aluminate

Table 2 Results of isotherm parameters and error functions obtained in the adsorption of MB onto *Ob*L-ZnONp

Isotherms	Parameters	R^2	SSE	SAE	ARE	HYBRID	MPSD	X^2
Freundlich	k_F = 3.64 $1/n$ = 0.446	0.991	2.97	2.99	5.70	0.31	0.944	0.243
Langmuir	k_L = 0.146 R_L = 0.242 q_{max} = 21.41	0.969	9.14	6.54	22.00	8.59	0.976	1.33
Temkin	B_T = 0.703 k_T = 3.157	0.920	14.03	8.35	34.30	9.28	0.977	3.06
Dubinin-Radushkevich	k_D = 0.145 q_s = 10.26 E = 1.857	0.551	127.77	21.01	49.90	16.45	0.982	11.31

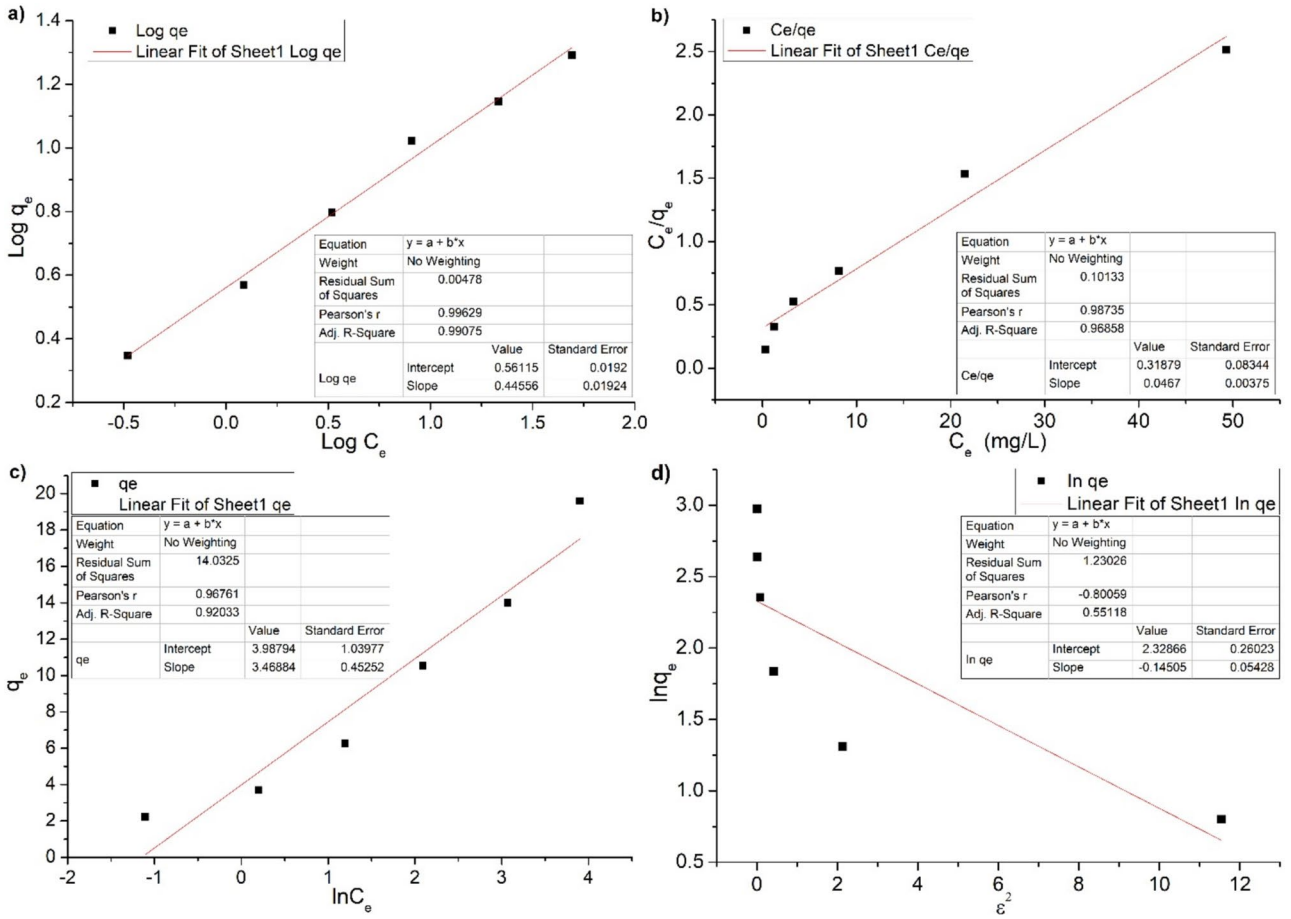


Fig. 10 Linear regression curves for a-Freundlich, b-Langmuir, c-Temkin, d-Dubinin–Redushkevich models

nanoparticles (Ismail et al. 2013). In addition, in a study, MB dye removal was performed using ZnNps synthesized from sawdust waste. In that study, it was reported that higher results were achieved in the basic part with increasing pH value (Oyewo et al. 2020).

Effect of initial adsorbent amount In order to achieve optimum removal efficiency, the variability in the amount of *Ob*L-ZnONp needs to be determined. In this context, the results obtained from the experiments conducted with *Ob*L-ZnONp in amounts ranging from 0.0312 g/L to 1.25 g/L are presented in Fig. 5.

According to Fig. 4, when 0.3125 mg *Ob*L-ZnONp was added to 10 mL volume MB dye with a concentration of 1 mg/L, the removal rate was obtained as 32.61%, while when the amount of *Ob*L-ZnONp was increased to 2.5 mg, the removal efficiency reached 69.57%, and finally when the amount of *Ob*L-ZnONp was added as 7.5 mg, the removal rate was obtained as 100%. On the other hand, while the q_e amount was 0.96 mg/g at the lowest *Ob*L-ZnONp amount, it was seen that the q_e amount decreased when the dosage amount was increased. Accordingly, it is quite natural

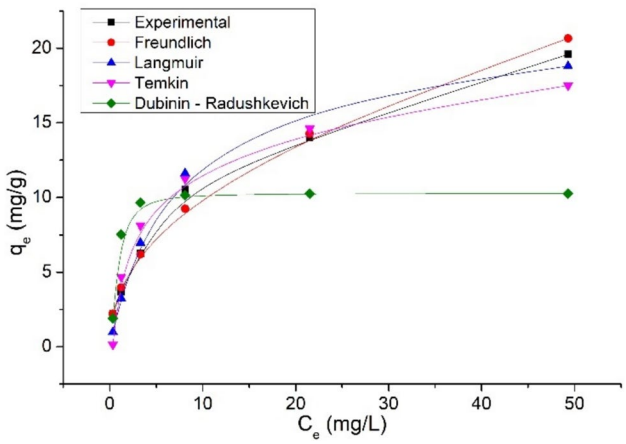


Fig. 11 Plot of q_e values of each isotherm model and laboratory results against C_e value

that the removal efficiency increased due to the increase in active surface areas with the increase in the amount of *Ob*L-ZnONp. When the literature was examined, it was reported that the removal efficiency increased with the increase in the

amount of adsorbent in the adsorption of MB dye onto gum ghatti/TiO_2 nanoparticles (Mittal and Ray 2016).

Effect of time Determination of contact time is very important in the adsorption process. In this context, the results obtained in the experimental study by adding 0.75 mg *Ob*L-ZnONp to the solution with 1 mg/L MB concentration in 50 mL solution volume are presented in Fig. 6.

In Fig. 6, the removal rate was obtained as 22.8% in the 1st minute, while the rate reached 64.1% in the 1st minute and exceeded 90.2% in the 4th minute. It is clear that there is an increase in removal efficiency with increasing reaction time, but a decrease in removal rate is observed. This situation can be explained by the decrease in the active sites on the *Ob*L-ZnONp molecules. When the literature is examined, it is reported that around 90% MB dye removal was achieved in the 10th minute in the adsorption of MB dye with magnesium silicate hydrate NPs. (Huang et al. 2018).

Effect of initial concentration The capacity of the adsorbent is determined by determining the effect of the change in the initial pollutant concentration. In this context, the data obtained from the experiment carried out by adding MB dye in increasing concentrations between 2 and 64 mg/L to 6 different test tubes, each with 1 g/L *Ob*L-ZnONp and a volume of 10 mL, are shown in Fig. 7.

When the figure is examined, the efficiency is 83.5% when the initial dye concentration is 2 mg/L. However, when the initial concentration was 8 mg/L, a decrease in efficiency was detected and measured as 49.38%. On the other hand, when the dye concentration reached 64 mg/L, the efficiency decreased significantly and fell to 22.97%. On the other hand, at the initial dye concentrations of 2, 8 and 64 mg/L, the q_e values were calculated as 2.23, 3.71 and 19.60. Accordingly, as the concentration of MB dye in the solution increased, the removal efficiency appeared to decrease since the active site on the *Ob*L-ZnONp pores became saturated, but the q_e value increased. In the literature, it has been reported that a similar decrease in the removal efficiency was observed with the increase in the initial dye concentration in MB dye removal with $MgFe_2O_4$ nanoparticles (Al-Wasidi et al. 2023). It was reported that similar results were obtained in a different study in which pine cone powders were used as biosorbent and adsorption tests of 2 dyes (MB and Eriochrome Black T) were performed (Solmaz 2024).

Table 3 Results of calculated thermodynamic parameters on the adsorption of MB dye onto *Ob*L-ZnONp

Temp. (K)	K_L	ΔG° (KJ/mol)	ΔH° (KJ/mol)	ΔS° (J/Kmol)	R^2
298	0.500	1.717	−7.69	−31.60	0.996
308	0.446	2.068			
318	0.411	2.348			

Adsorption kinetics

The values obtained in the adsorption experiments conducted in the laboratory studies were tried to be interpreted from a kinetic perspective. It is tried to provide information about the adsorption performance of MB dye on

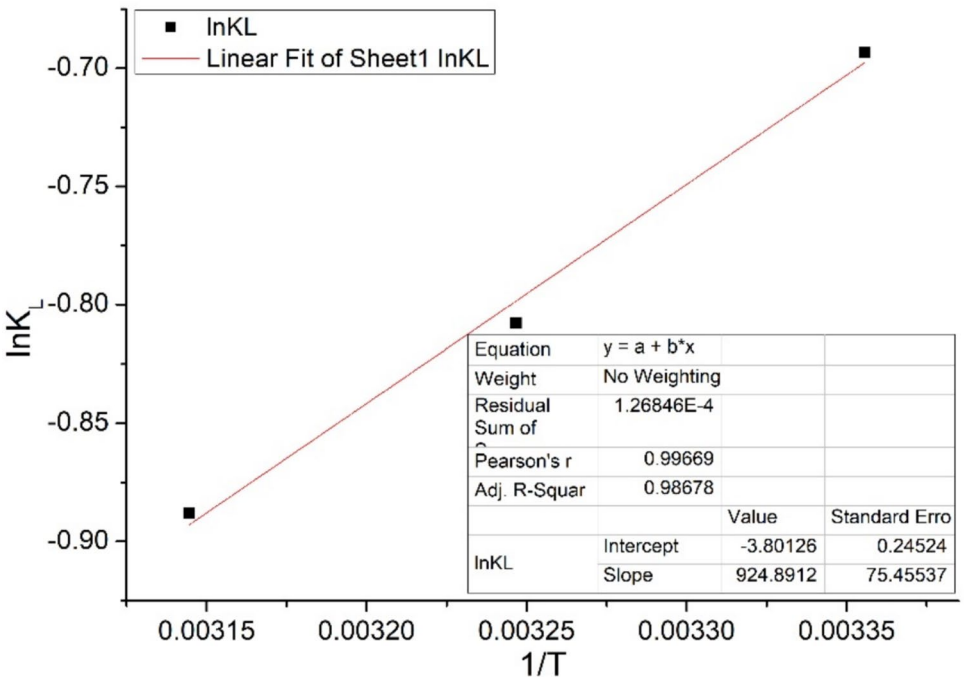


Fig. 12 Plot of $1/T$ versus $\ln K_L$ in the adsorption of MB dye onto *Ob*L-ZnONp

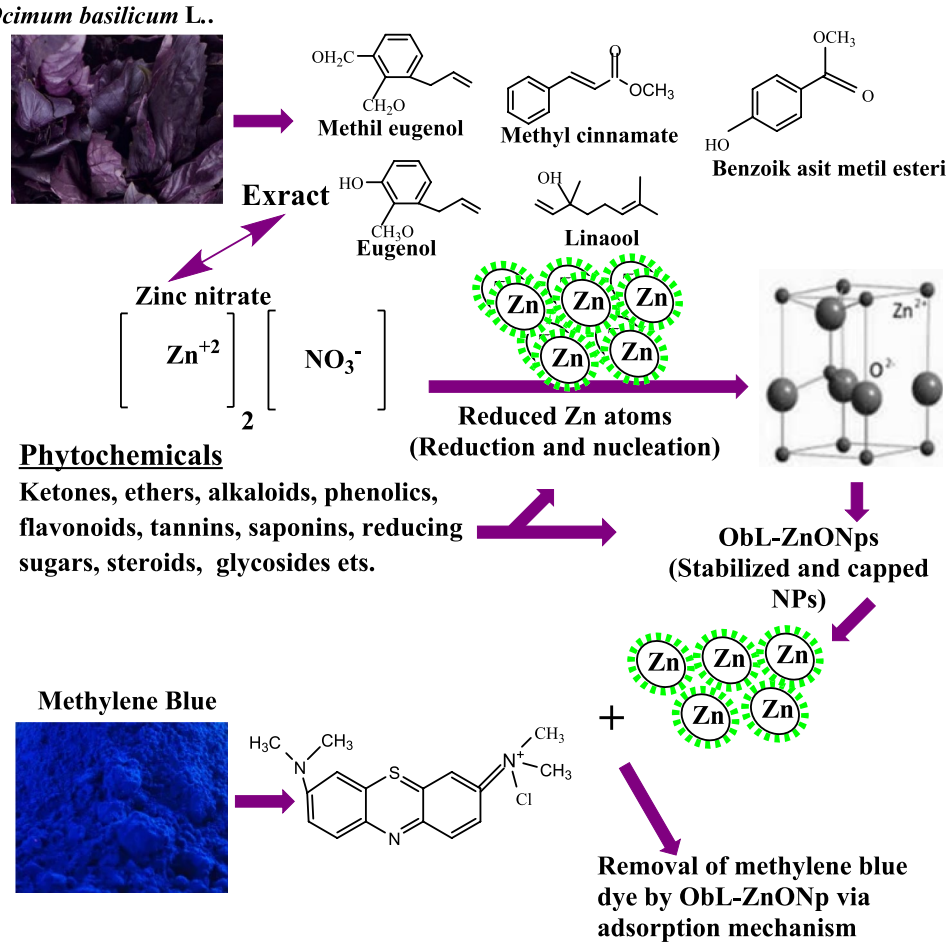


Fig. 13 *Ob*L-ZnONp synthesis and MB dye removal mechanism

*Ob*L-ZnONp and the removal mechanism. In this process, which is generally known to occur in 3 stages, in the first stage, the 'External diffusion' stage, the pollutant passes through the liquid film layer covering the outer part of the adsorbent. Here, the difference between the concentration of the solution and the surface concentration of the adsorbent is expressed as the driving force of External diffusion. After this stage, the second stage, the "internal diffusion" stage, comes, where the pollutant diffuses into the pores of the adsorbent. The last stage is defined as "adsorbate in the active sites", where the pollutant adsorbs into the active sites of the adsorbent in the third stage(Qiu et al. 2009; Wang and Guo 2020; Revellame et al. 2020). Four different kinetic models were tried in this study. The models are listed below;

PFO kinetic model;

The modeling nonlinear form is presented in Eq. (9) (Lagergren 1898).

$$\frac{dq_t}{d_t} = K_1(q_e - q_t) \tag{9}$$

Here the q term represents the amount of pollutant (mg/L) adsorbed by the unit solid (m). The q_e term represents the removal rate at the equilibrium time, and the q_t term represents the removal rate at any time t. In addition, the K_1 term is the constant of the PFO kinetic model (1/min).

PSO kinetic model;

The formula of the model is presented in Eq. (10) (Ho et al. 1996).

$$\frac{dq_t}{d_t} = K_2(q_e - q_t)^2 \tag{10}$$

Here, the K_2 term is the constant of the PSO kinetic model (1/min).

Elovich kinetic model;

The formula of the model is presented in Eq. (11) (Kumar et al. 2011).

$$q_t = \frac{1}{\beta}\ln(\alpha\beta) + \frac{1}{\beta}\ln t \tag{11}$$

Here, α is the expression of the initial adsorption rate (mg/g), and β is the constant value of the desorption that took place (g/mg).

Intra-particle diffusion model;

Table 4 Comparison of the results obtained in experimental studies with the literature

	This study	Kaur et al. (2021)	Cheng et al. (2020)	El-Ghobashy et al. (2023)	Aaddouz et al. (2023)	Kataria et al. (2016)	Mahmoodi et al. (2014)
NP chemical	ZnO	ZnO	Cellulose asetate	Mn + Fe + Mn	Hydroxyapatite	Zn and Ag	Amino silica
NP origin	*Ocimum Basilicum*	–	–	–	–	Cotton fibers	–
Experiment volume (mL)	10	20	20	50	10	100	250 mL
Mixing speed (rpm)	200	350	–	140	–	50–250	200
Experiment time (min)	0–30	10–40	30 h	–	5–120	15–120	60
Working pH's	3–11	2–12	2–10	4–12	6–12	2–10	2, 5, 8, and 10
Optimum pH	7.00	3	6.5	6.13	–	6.0	2
Working temp. (°C)	25, 35, 45	25	25, 35, 45	25–50	25–60	10–70	25
Optimum temp. (°C)	25	–	25	30	25	27.1	–
Initial conc. (mg/L)	2–64	6–30	50	12.71	5–90	10–100	25, 50, 75, and 100
Adsorbent amount (g/L)	0.0312–1.25	0.5–7.5	0.02	0.10–0.30	1.0	0.2–1.0	0.01–0.07 g
Pollutant type	MB	Eriochrome black T	MB	MB	MB	Victoria Blue B	4 dye[a]
q_{max} (mg/g)	21.41	49.30–73.95	96.9	89.63	38.39	163.93	37.45–113.64

[a]Acid blue 92, Direct Black 22, Direct Red 31, Direct Red 80

The equation of the model is presented in equation number 12 (Boyd et al. 1947).

$$q_t = K_{id}t^{1/2} + C \tag{12}$$

Here the K_{id} is model constant. K_{id} is obtained by plotting the value of $t^{1/2}$ against the value of q_t in the equation.

The summary of the results obtained from the kinetic models is illustrated in Table 1. In addition, graphs showing linear regression curves of each model are presented in Fig. 8. In addition, the q_e value for time is given in Fig. 9.

When the obtained values are examined, the correlation coefficients (R^2) values of the Intra-Particle Diffusion, Elovich and PFO models were found as 0.654, 0.905 and 0.906, respectively, while the R^2 value of the PSO model was found as 0.999. Also, when the error functions between the data obtained from the laboratory values and the values obtained from the models are examined, the SSE, SAE and ARE values were calculated as 0.02, 0.332 and 8.49, respectively, while the HYBRID, MPSD and X^2 values were calculated as 6.37, 0.972 and 0.046. When evaluated in terms of error functions according to the table, it is seen that the most suitable model is PSO. When looking at the literature, it has been reported that the PSO model is suitable for the adsorption of Malachite green ($R^2 \geq 0.996$) and Congo red ($R^2 \geq 0.967$) dyes with Fe–Zn nanoparticles (Gautam et al. 2015). Similarly, it has been reported that the PSO model is suitable for the removal of Victoria Blue B dye with ZnNPs obtained from flowers with a value of R^2: 0.997 (Kataria et al. 2016).

Adsorption isotherms

It is used to define the possible relationship between the remaining pollutant (MB) concentration in the solution at the equilibrium state of the experiment and the adsorbent substance (*Ob*L-ZnONp) we use by interpreting the results obtained from the adsorption isotherms. Thus, the pollutant adsorption capacity of the *Ob*L-ZnONp surface is determined thanks to its specific properties and affinity. Many isotherms are used to determine whether this

short-term is mono-component or different (Ali et al. 2018). In this context, 4 different isotherms were tested and compared with each other.

Freundlich isotherm model;

The equation of the model is presented in Eq. (13) (Freundlich 1906; Jeppu and Clement 2012).

$$q_e = K_F C_e^{1/n} \tag{13}$$

Here, q_e value represents the amount of MB adsorbed by *Ob*L-ZnONp at equilibrium (mg/g). Also, K_F and n terms are defined as model constants. On the other hand, and C_e value is the concentration of MB dye remaining in the solution at equilibrium (mg/L).

Langmuir isotherm model;

The equation of the model is presented in Eq. (14), and the equation of the dispersion constant is presented in Eq. (15) (Gerente et al. 2007).

$$q_e = \frac{q_{max} K_L C_e}{1 + K_L C_e} \tag{14}$$

$$R_L = \frac{1}{1 + a_L C_e} \tag{15}$$

Here, R_L is the dispersion constant, K_L and a_L are model constants.

Temkin isotherm model;

The model equation is displayed in Eq. (16) (Allen et al. 2004).

$$q_e = B ln(A_T C_e) \text{ and } B = \frac{RT}{b_T} \tag{16}$$

Here, B, R, T and b_T are expressed as cautious constant (J/mol), universal gas constant (8.314 j/mol.K), temperature (K) and heat of isotherm constant (kJ/mol), respectively.

Dubinin–Redushkevich isotherm model;

Model equation is given in Eq. (17) (Hu and Zhang 2019).

$$q_e = q_m \exp(-Be^2) \text{ and } e = RTln\left(1 + \frac{1}{C_e}\right) \tag{17}$$

Here e term presented here, unlike other models, is the Polanyi potential.

The summary of the results obtained from the isotherm models is presented in Table 2. In addition, the graphs obtained from the linear regression curves of the models are given in Fig. 10. In addition, the graph drawn for the q_e value obtained from experiments and models against the concentration of the MB dye remaining in the solution (C_e) is given in Fig. 11.

According to the table, the R^2 values of Dubinin-Radushkevich, Temkin and Langmuir isotherm models were obtained as 0.551, 0.920 and 0.969, respectively, while the R^2 value of the Freundlich isotherm model was obtained as 0.991. When the error functions are compared in the isotherm models as in the kinetic models, it is seen that the lowest values are in the Freundlich isotherm model. Accordingly, the adsorption of MB dye onto *Ob*L-ZnONp is suitable for the Freundlich model. The Freundlich isotherm model was used from the graph of $\ln C_e$ versus $\ln q_e$. In addition, the $1/n$ and k_F values obtained from this graph define the efficiency of adsorption and the degree of heterogeneity. Since the k_F value is less than 1 here, it can be said that the adsorption occurs chemically. It can also be interpreted that a multilayer adsorption mechanism dominates and the active sites on the adsorbent surface have a heterogeneous distribution (Foo and Hameed 2010). Similarly, it has been reported in the literature that Brilliant Blue R dye obeys the Freundlich isotherm with R^2 0.970 in the adsorption of composite ZnO NP (Reghioua et al. 2021), and with R^2 0.922 in the adsorption of Pb ions (Ali et al. 2018).

Adsorption thermodynamic and mechanism

By evaluating the adsorption mechanism from a thermodynamic perspective, information is obtained about the progress of the reaction and whether it has a heat-receiving or heat-releasing mechanism. To determine this, experiments were conducted at temperatures of 298, 308 and 318. From the numerical data obtained as a result of the experiment, Eq. (18) was used to calculate the Gibbs free energy changes (ΔG°). Also, Eqs. (19) and (20) were used to determine the enthalpy (ΔH°) and entropy (ΔS°) parameters.

$$\Delta G = -RTLnK \tag{18}$$

$$\Delta G^\circ = \Delta H^\circ - T\Delta S^\circ \tag{19}$$

$$\text{Ln}K = \frac{\Delta S}{R} - \frac{\Delta H}{RT} \tag{20}$$

In addition, the graph obtained from the K_L value against the $1/T$ value is presented in Fig. 12, and the general summary of the thermodynamic results is presented in Table 3.

In addition, the diagram created for the production and removal mechanism is displayed in Fig. 13. When the data obtained from the graphs and tables are examined, a positive ΔG° value means that the reaction occurs physically. According to the results, if the ΔG° value is negative, it means that the reaction is spontaneous, and if it is positive, it means that the reaction is not spontaneous (Al-Aoh et al. 2020). In addition, as can be seen, the ΔH° values are negative, and the negative value of this value means that the adsorption of MB dye onto *Ob*L-ZnONp is an exothermic process. Physical adsorption (Van der Waals interactions) is lower than 20 kJ/mol (Peres et al. 2018).

Desorption and reusability test

Desorption and reusability studies were conducted at room temperature (23 ± °C) and pH 7. Initial MB concentration was 10 mg/L and 10 mL volume tubes were used. *Ob*L-ZnONp was added to the tubes to be 1 g/L. At the end of the experiment, centrifugation was performed and the MB dye concentration in the upper phase water was measured. 10 mL of 0.1 M HCl was added to the pellet remaining at the bottom of the tube and left to shake, aiming to remove the MB dye from *Ob*L-ZnONp. At the end of the process, centrifugation was performed and the upper phase liquid was discarded. The remaining pellet was washed with distilled water and centrifuged again and the upper phase liquid was discarded. Again, MB with a concentration of 10 mg/L was added to the remaining pellet and left to shake, centrifugation was performed at the end of the period and the MB concentration in the upper phase liquid was measured. The cycles followed each other in this way. While the removal efficiency was 96% in the 1st cycle, the efficiency decreased to 71% in the 2nd cycle and finally, the efficiency was calculated as 65% in the 3rd cycle. There may be 2 possible reasons for the decrease in the removal efficiency. The first is the degrading effect of the washing solution on the nanoparticles. The second may be due to the mass loss in ObL-ZnONp at the end of each process cycle. When the literature is examined, it was reported that a desorption efficiency of 96–90% was achieved in a study conducted with Acid Blue 2, Direct Red 23 and Direct Red dyes with ZnONp (Mahmoodi and Najafi 2012). In a different study, MB and Brilliant green dyes were removed in dye removal studies conducted with F_3O_4 loaded activated carbon nanoparticles, and it was reported that an efficiency of over 70% was achieved in the 2nd cycle, while a desorption efficiency of around 60% was achieved in the 3rd cycle (Joshi et al. 2019).

Comparison of the results obtained in experimental studies with the literature

The results obtained in experimental studies and the results in the literature are presented in Table 4. Accordingly, in a study where MB dye was removed with nanoparticles produced using Cellulose acetate, screenings were performed in the pH range of 2–10 and the optimum pH was determined to be 6.5 and the q_{max} value was reported to be 96.9 mg/g (Cheng et al. 2020). Also, at the different study where MB dye was treated with Hydroxyapatite-based Np, it was reported that 38.39 mg/g adsorbent capacity was reached at the end of the 120-min experiment (Aaddouz et al. 2023). On the other hand, at the different work where Zn/Ag-Np based on cotton fibers were produced, Victoria Blue B dye was removed and it was reported that 163.93 mg/g removal rate was achieved in the removal studies using Np at a concentration of 0.2–1 g/L (Kataria et al. 2016). Also, in dye removal works with Np synthesized with amio silica, experiments were carried out at different pH and initial concentrations. Also, it was reported that the produced adsorbent was effective in dye removal (Mahmoodi et al. 2014). In this study, MB dye removal studies with Np obtained from *Ocimum Basilicum* wastes contributed to the literature.

Conclusion

The results obtained in the adsorption of toxic MB dye with *Ob*L-ZnONp obtained by the green synthesis method are listed as follows;

- The effects of varying pH, amount of *Ob*L-ZnONp, reaction time, initial dye concentration and temperature change were studied.
- Four different kinetic (PFO, PSO, Elovich and Intraparticle diffusion) and 4 isotherm models (Freundlich, Langmuir, Temkin and Dubinin-Radushkevich) were tested.
- SSE, SAE, ARE, HYBRID, MPSD and X^2 error functions were used to determine the optimum kinetic and isotherm model.
- The most suitable kinetic model was determined as PSO with an R^2 value of 0.999. In addition, the most suitable

isotherm model was determined as Freundlich with an R^2 value of 0.991.
- The characteristic structures of both raw and MB-loaded *Ob*L-ZnONps were determined by FTIR and SEM–EDX analyses.
- It was determined that the adsorption mechanism was an exothermic process.
- While the removal efficiency was determined as 22.8%, 64.1% and 90.2% at 30, 60 and 240 s, the adsorption process was completed after 15 min.
- In desorption tests, 65% efficiency was obtained in the 3rd cycle.
- The amount of MB removed by unit *Ob*L-ZnONp was calculated as 21.41 mg/g.

This study proved that *Ob*L-ZnONp synthesized from wastes removes MB cheaply and rapidly.

Acknowledgements The authors would like to thank to their university for support.

Author contributions Talip Turna: Conceptualization, formal analysis, investigation, data curation, writing—original draft. Alper Solmaz: Conceptualization, data curation, result interpretation, writing—review & editing. Ayşe Baran: Original draft, formal analysis, data curation, writing—review & editing.

Funding Open access funding provided by the Scientific and Technological Research Council of Türkiye (TÜBİTAK). No funding.

Data availability The datasets generated during and/or analyzed during the current study are available from the corresponding author on reasonable request.

Declarations

Conflict of interest The authors declare that they have no known competing financial interests or personal relationships that could have appeared to influence the work reported in this paper.

Ethical approval Not applicable.

Consent to participate All authors have given consent to their contribution.

Consent for publication All authors have agreed with the content and all have given explicit consent to publish.

Open Access This article is licensed under a Creative Commons Attribution 4.0 International License, which permits use, sharing, adaptation, distribution and reproduction in any medium or format, as long as you give appropriate credit to the original author(s) and the source, provide a link to the Creative Commons licence, and indicate if changes were made. The images or other third party material in this article are included in the article's Creative Commons licence, unless indicated otherwise in a credit line to the material. If material is not included in the article's Creative Commons licence and your intended use is not permitted by statutory regulation or exceeds the permitted use, you will need to obtain permission directly from the copyright holder. To view a copy of this licence, visit http://creativecommons.org/licenses/by/4.0/.

References

Aaddouz M, Azzaoui K, Akartasse N et al (2023) Removal of methylene blue from aqueous solution by adsorption onto hydroxyapatite nanoparticles. J Mol Struct 1288:135807. https://doi.org/10.1016/j.molstruc.2023.135807

Abdelsattar AS, Kamel AG, Hussein AH et al (2023) The promising antibacterial and anticancer activity of green synthesized zinc nanoparticles in combination with silver and gold nanoparticles. J Inorg Organomet Polym Mater 33:1868–1881. https://doi.org/10.1007/s10904-023-02614-y

Aiman Khan S, Jain M, Pandey A et al (2022) Leveraging the potential of silver nanoparticles-based materials towards sustainable water treatment. J Environ Manage 319:115675. https://doi.org/10.1016/j.jenvman.2022.115675

Al-Aoh HA, Mihaina IAM, Alsharif MA et al (2020) Removal of methylene blue from synthetic wastewater by the selected metallic oxides nanoparticles adsorbent: equilibrium, kinetic and thermodynamic studies. Chem Eng Commun 207:1719–1735. https://doi.org/10.1080/00986445.2019.1680366

Albarakaty FM, Alzaban MI, Alharbi NK et al (2023) Zinc oxide nanoparticles, biosynthesis, characterization and their potent photocatalytic degradation, and antioxidant activities. J King Saud Univ Sci 35:102434. https://doi.org/10.1016/j.jksus.2022.102434

Al-darwesh MY, Ibrahim SS, Hamid LL (2024) Ficus carica latex mediated biosynthesis of zinc oxide nanoparticles and assessment of their antibacterial activity and biological safety. Nano-Struct Nano-Objects 38:101163. https://doi.org/10.1016/j.nanoso.2024.101163

Ali A, Mannan A, Hussain I et al (2018) Effective removal of metal ions from aquous solution by silver and zinc nanoparticles functionalized cellulose: isotherm, kinetics and statistical supposition of process. Environ Nanotechnol Monit Manag 9:1–11. https://doi.org/10.1016/J.ENMM.2017.11.003

Allen SJ, Mckay G, Porter JF (2004) Adsorption isotherm models for basic dye adsorption by peat in single and binary component systems. J Colloid Interface Sci 280:322–333. https://doi.org/10.1016/j.jcis.2004.08.078

Al-Wasidi AS, Algethami FK, Saad FA, Abdelrahman EA (2023) Remarkable high adsorption of methylene blue dye from aqueous solutions using facilely synthesized $MgFe_2O_4$ nanoparticles. J Inorg Organomet Polym Mater 33:2035–2045. https://doi.org/10.1007/s10904-023-02652-6

Amin ZS, Afzal M, Ahmad J et al (2023) Synthesis, characterization and biological activities of zinc oxide nanoparticles derived from secondary metabolites of lentinula edodes. Molecules 28:1–17. https://doi.org/10.3390/molecules28083532

Boyd GE, Adamson AW, Myers LS (1947) The exchange adsorption of ions from aqueous solutions by organic zeolites. II. Kinetics. J Am Chem Soc 69:2836–2848. https://doi.org/10.1021/JA01203A066/ASSET/JA01203A066.FP.PNG_V03

Chandra H, Kumari P, Bontempi E, Yadav S (2020) Medicinal plants: treasure trove for green synthesis of metallic nanoparticles and their biomedical applications. Biocatal Agric Biotechnol 24:1878–8181. https://doi.org/10.1016/j.bcab.2020.101518

Chaudhary J, Tailor G, Yadav M, Mehta C (2023) Green route synthesis of metallic nanoparticles using various herbal extracts: a review. Biocatal Agric Biotechnol 50:1878–8181. https://doi.org/10.1016/j.bcab.2023.102692

Cheng J, Zhan C, Wu J et al (2020) Highly efficient removal of methylene blue dye from an aqueous solution using cellulose acetate nanofibrous membranes modified by polydopamine. ACS Omega 5:5389–5400. https://doi.org/10.1021/ACSOMEGA.9B04425/ASSET/IMAGES/MEDIUM/AO9B04425_M013.GIF

El-Ghobashy MA, Salem IA, El-Dahrawy WM, Salem MA (2023) Fabrication of α-MnO2/Fe-Mn binary oxide nanocomposite as an efficient adsorbent for the removal of methylene blue from wastewater. J Mol Struct 1272:134118. https://doi.org/10.1016/J.MOLSTRUC.2022.134118

Elsamra RMI, Masoud MS, Zidan AA et al (2024) Green synthesis of nanostructured zinc oxide by Ocimum tenuiflorum extract: characterization, adsorption modeling, cytotoxic screening, and metal ions adsorption applications. Biomass Convers Biorefin 14:16843–16856. https://doi.org/10.1007/s13399-022-03709-1

Foo KY, Hameed BH (2010) Insights into the modeling of adsorption isotherm systems. Chem Eng J 156:2–10. https://doi.org/10.1016/J.CEJ.2009.09.013

Freundlich HMF (1906) Over the adsorption in solution. J Phys Chem 57:1100–1107

Gautam RK, Rawat V, Banerjee S et al (2015) Synthesis of bimetallic Fe–Zn nanoparticles and its application towards adsorptive removal of carcinogenic dye malachite green and Congo red in water. J Mol Liq 212:227–236. https://doi.org/10.1016/J.MOLLIQ.2015.09.006

Gerente C, Lee VKC, Le CP, McKay G (2007) Application of chitosan for the removal of metals from wastewaters by adsorption—mechanisms and models review. Crit Rev Environ Sci Technol 37:41–127. https://doi.org/10.1080/10643380600729089

Gómez-Pastora J, Bringas E, Ortiz I (2014) Recent progress and future challenges on the use of high performance magnetic nano-adsorbents in environmental applications. Chem Eng J 256:187–204. https://doi.org/10.1016/j.cej.2014.06.119

Ho YS, Wase' D, Forster CF (1996) Removal of lead ions from aqueous solution using sphagnum moss peat as adsorbent. Water SA 22:214–219

Hole G, Hole AS (2019) Recycling as the way to greener production: a mini review. J Clean Prod 212:910–915. https://doi.org/10.1016/j.jclepro.2018.12.080

Hu Q, Zhang Z (2019) Application of Dubinin-Radushkevich isotherm model at the solid/solution interface: a theoretical analysis. J Mol Liq 277:646–648. https://doi.org/10.1016/j.molliq.2019.01.005

Huang R, He L, Zhang T et al (2018) Fabrication and adsorption behavior of magnesium silicate hydrate nanoparticles towards methylene blue. Nanomaterials 8:271. https://doi.org/10.3390/nano8050271

Ismail B, Hussain ST, Akram S (2013) Adsorption of methylene blue onto spinel magnesium aluminate nanoparticles: adsorption isotherms, kinetic and thermodynamic studies. Chem Eng J 219:395–402. https://doi.org/10.1016/j.cej.2013.01.034

Jamkhande PG, Ghule NW, Bamer AH, Kalaskar MG (2019) Metal nanoparticles synthesis: an overview on methods of preparation, advantages and disadvantages, and applications. J Drug Deliv Sci Technol 53:101174. https://doi.org/10.1016/j.jddst.2019.101174

Jeppu GP, Clement TP (2012) A modified Langmuir-Freundlich isotherm model for simulating pH-dependent adsorption effects. J Contam Hydrol 129–130:46–53. https://doi.org/10.1016/J.JCONHYD.2011.12.001

Joshi S, Garg VK, Kataria N, Kadirvelu K (2019) Applications of Fe3O4@AC nanoparticles for dye removal from simulated wastewater. Chemosphere 236:124280. https://doi.org/10.1016/j.chemosphere.2019.07.011

Kataria N, Garg VK, Jain M, Kadirvelu K (2016) Preparation, characterization and potential use of flower shaped Zinc oxide nanoparticles (ZON) for the adsorption of Victoria Blue B dye from aqueous solution. Adv Powder Technol 27:1180–1188. https://doi.org/10.1016/J.APT.2016.04.001

Kaur Y, Jasrotia T, Kumar R et al (2021) Adsorptive removal of eriochrome black T (EBT) dye by using surface active low cost zinc oxide nanoparticles: a comparative overview. Chemosphere 278:130366. https://doi.org/10.1016/J.CHEMOSPHERE.2021.130366

Kaval U, Hoşgören H (2024) Biosynthesis, Characterization, and biomedical applications of gold nanoparticles with Cucurbita moschata duchesne ex poiret peel aqueous extracts. Molecules 29:923. https://doi.org/10.3390/molecules29050923

Kumar PS, Ramalingam S, Kirupha SD et al (2011) Adsorption behavior of nickel(II) onto cashew nut shell: equilibrium, thermodynamics, kinetics, mechanism and process design. Chem Eng J 167:122–131. https://doi.org/10.1016/J.CEJ.2010.12.010

Lagergren SK (1898) About the theory of so-called adsorption of soluble substances. Sven Vetenskapsakad Handingarl 24:1–39

Lellis B, Zani Fávaro-Polonio C, Pamphile JA, Polonio JC (2019) Effects of textile dyes on health and the environment and bioremediation potential of living organisms. Biotechnol Res Innov 3:275–290. https://doi.org/10.1016/j.biori.2019.09.001

Madhumitha G, Elango G, Roopan SM (2016) Biotechnological aspects of ZnO nanoparticles: overview on synthesis and its applications. Appl Microbiol Biotechnol 100:571–581. https://doi.org/10.1007/s00253-015-7108-x

Mahmoodi NM, Najafi F (2012) Preparation of surface modified zinc oxide nanoparticle with high capacity dye removal ability. Mater Res Bull 47:1800–1809. https://doi.org/10.1016/j.materresbull.2012.03.026

Mahmoodi NM, Maghsoudi A, Najafi F et al (2014) Primary–secondary amino silica nanoparticle: synthesis and dye removal from binary system. Desalin Water Treat 52:7784–7796. https://doi.org/10.1080/19443994.2013.833872

Manojkumar U, Kaliannan D, Srinivasan V et al (2023) Green synthesis of zinc oxide nanoparticles using Brassica oleracea var. botrytis leaf extract: photocatalytic, antimicrobial and larvicidal activity. Chemosphere 323:138263. https://doi.org/10.1016/j.chemosphere.2023.138263

Mittal H, Ray SS (2016) A study on the adsorption of methylene blue onto gum ghatti/TiO_2 nanoparticles-based hydrogel nanocomposite. Int J Biol Macromol 88:66–80. https://doi.org/10.1016/j.ijbiomac.2016.03.032

Nandan P, Ajithkumar A, Siddiqui SA et al (2023) Sustainable application of nanoparticles in wastewater treatment: fate, current trend & paradigm shift. Environ Res. https://doi.org/10.1016/j.envres.2023.116071

Ncibi MC (2008) Applicability of some statistical tools to predict optimum adsorption isotherm after linear and non-linear regression analysis. J Hazard Mater 153:207–212. https://doi.org/10.1016/J.JHAZMAT.2007.08.038

Ocsoy I, Tasdemir D, Mazicioglu S et al (2017) Biomolecules incorporated metallic nanoparticles synthesis and their biomedical applications. Mater Lett 212:45–50. https://doi.org/10.1016/j.matlet.2017.10.068

Omran AME (2023) Characterization of green route synthesized zinc oxide nanoparticles using Cyperus rotundus rhizome extract: antioxidant, antibacterial, anticancer and photocatalytic potential. J Drug Deliv Sci Technol 79:104000. https://doi.org/10.1016/j.jddst.2022.104000

Oyewo OA, Adeniyi A, Sithole BB, Onyango MS (2020) Sawdust-based cellulose nanocrystals incorporated with ZnO nanoparticles as efficient adsorption media in the removal of methylene blue dye. ACS Omega 5:18798–18807. https://doi.org/10.1021/acsomega.0c01924

Peres EC, Slaviero JC, Cunha AM et al (2018) Microwave synthesis of silica nanoparticles and its application for methylene blue adsorption. J Environ Chem Eng 6:649–659. https://doi.org/10.1016/j.jece.2017.12.062

Perveen R, Shujaat S, Qureshi Z et al (2020) Green versus sol-gel synthesis of ZnO nanoparticles and antimicrobial activity evaluation against panel of pathogens. J Market Res 9(4):7817–7827. https://doi.org/10.1016/j.jmrt.2020.05.004

Ponnusami V, Madhuram R, Krithika V, Srivastava SN (2008) Effects of process variables on kinetics of methylene blue sorption onto untreated guava (Psidium guajava) leaf powder: statistical analysis. Chem Eng J 140:609–613. https://doi.org/10.1016/j.cej.2007.11.003

Punia P, Kumar Bharti M, Chalia S et al (2021) Recent advances in synthesis, characterization, and applications of nanoparticles for contaminated water treatment—a review. Ceram Int 47:1526–1550. https://doi.org/10.1016/j.ceramint.2020.09.050

Qiu H, Lv L, Pan BC et al (2009) Critical review in adsorption kinetic models. J Zhejiang Univ Sci A 10:716–724. https://doi.org/10.1631/JZUS.A0820524

Reghioua A, Barkat D, Jawad AH et al (2021) Magnetic chitosan-glutaraldehyde/zinc oxide/Fe3O4 nanocomposite: optimization and adsorptive mechanism of remazol brilliant blue R dye removal. J Polym Environ 29:3932–3947. https://doi.org/10.1007/S10924-021-02160-Z/FIGURES/8

Revellame ED, Fortela DL, Sharp W et al (2020) Adsorption kinetic modeling using pseudo-first order and pseudo-second order rate laws: a review. Clean Eng Technol 1:100032. https://doi.org/10.1016/J.CLET.2020.100032

Russo V, Masiello D, Trifuoggi M et al (2016) Design of an adsorption column for methylene blue abatement over silica: From batch to continuous modeling. Chem Eng J 302:287–295. https://doi.org/10.1016/j.cej.2016.05.020

Said HA, Bourhim IA, Ouarga A et al (2023) Sustainable phosphorylated microcrystalline cellulose toward enhanced removal performance of methylene blue. Int J Biol Macromol 225:1107–1118. https://doi.org/10.1016/j.ijbiomac.2022.11.172

Salem SS, EL-Belely EF, Niedbała G et al (2020) Bactericidal and ın-vitro cytotoxic efficacy of silver nanoparticles (Ag-NPs) fabricated by endophytic actinomycetes and their use as coating for the textile fabrics. Nanomaterials 10:1–20. https://doi.org/10.3390/nano10102082

Shaban AS, Owda ME, Basuoni MM et al (2024) Punica granatum peel extract mediated green synthesis of zinc oxide nanoparticles: structure and evaluation of their biological applications. Biomass Convers Biorefin 14:12265–12281. https://doi.org/10.1007/s13399-022-03185-7

Shaghaghi Z, Mollaei S, Amani-Ghadim AR, Abedini Z (2023) Green synthesis of ZnO nanoparticles using the aqueous extract of Platanus orientalis: structural characterization and photocatalytic activity. Mater Chem Phys 305:127900. https://doi.org/10.1016/J.MATCHEMPHYS.2023.127900

Shah IA, Bilal M, Almanassra IW, Ihsanullah I (2024) A comprehensive review of graphene oxide-based membranes for efficient dye removal from water sources. Sep Purif Technol 330:125277. https://doi.org/10.1016/j.seppur.2023.125277

Shochah QR, Jabir FA (2024) Green synthesis of Au/ZnO nanoparticles for anticancer activity and oxidative stress against MCF-7 cell lines. Biomass Convers Biorefin 14:15283–15296. https://doi.org/10.1007/s13399-022-03697-2

Solmaz A (2024) Adsorption of methylene blue and eriochrome black t onto pinecone powders (Pinus nigra Arn.): equilibrium, kinetics, and thermodynamic studies. Processes 12:2044. https://doi.org/10.3390/pr12092044

Solmaz A, Turna T, Baran A (2024) Removal of paracetamol from aqueous solution with zinc oxide nanoparticles obtained by green synthesis from purple basil (Ocimum basilicum L.) waste. Biomass Convers Biorefin. https://doi.org/10.1007/s13399-024-05355-1

Sreńscek-Nazzal J, Narkiewicz U, Morawski AW et al (2015) Comparison of optimized isotherm models and error functions for carbon dioxide adsorption on activated carbon. J Chem Eng Data 60:3148–3158. https://doi.org/10.1021/acs.jced.5b00294

Vidya C, Manjunatha C, Chandraprabha M et al (2017) Hazard free green synthesis of ZnO nano-photo-catalyst using Artocarpus Heterophyllus leaf extract for the degradation of Congo red dye in water treatment applications. J Environ Chem Eng 5:3172–3180. https://doi.org/10.1016/j.jece.2017.05.058

Villegas-Fuentes A, Garrafa-Gálvez HE, Quevedo-Robles RV et al (2023) Synthesis of semiconductor ZnO nanoparticles using Citrus microcarpa extract and the influence of concentration on their optical properties. J Mol Struct. https://doi.org/10.1016/j.molstruc.2023.135067

Wang J, Guo X (2020) Adsorption kinetic models: physical meanings, applications, and solving methods. J Hazard Mater 390:122156. https://doi.org/10.1016/J.JHAZMAT.2020.122156

Zhang X, Zhang P, Wu Z et al (2013) Adsorption of methylene blue onto humic acid-coated Fe_3O_4 nanoparticles. Colloids Surf A Physicochem Eng Asp 435:85–90. https://doi.org/10.1016/j.colsurfa.2012.12.056

Zhang C, Yin H, Bai X, Yang Z (2023) Ru doping induced lattice distortion of Cu nanoparticles for boosting electrochemical non-enzymatic hydrogen peroxide sensing. Colloids Surf A Physicochem Eng Asp 666:131311. https://doi.org/10.1016/J.COLSURFA.2023.131311

Authors and Affiliations

T. Turna[1] · A. Solmaz[2] · A. Baran[3]

✉ T. Turna
talipturna@gmail.com

[1] Department of Parks and Garden Plants-Diyarbakır Vocational School of Higher Education, Dicle University, Diyarbakır, Türkiye

[2] Department of Environmental Protection and Control-Iskenderun Vocational School of Higher Education, Iskenderun Technical University, Hatay, Turkey

[3] Department of Plant and Animal Production, Kızıltepe Vocational School, Mardin Artuklu University, Mardin, Turkey